Marine Geodesy, 26:117–127, 2003

0149-0419/03 $12.00 + .00
DOI: 10.1080/01490410390181234

Taylor & Francis
Taylor & Francis Group

Combining Lidar Elevation Data and IKONOS Multispectral Imagery for Coastal Classification Mapping

D. SCOTT LEE
JIE SHAN

Department of Geomatics Engineering
School of Civil Engineering
Purdue University
West Lafayette, Indiana, USA

This article studies the effect of airborne lidar (surface) elevation data on the classification of multispectral IKONOS images over a coastal area. The lidar data and IKONOS images are treated as independent multiple bands to conduct the classification. To do so, the lidar elevation data is first resampled to the same ground spacing interval and stretched to the same radiometric range as the IKONOS images. An unsupervised classification based on the ISODATA algorithm is then used to determine a class schema of six classes: road, water, marsh, roof, tree, and sand. Training sites and checking sites are selected over the lidar-IKONOS merged data set for the subsequent supervised classification and quality evaluation. The complete confusion matrices and average quality indices are presented to assess and compare the classification results. It is shown that the inclusion of the lidar elevation data benefits the separation of classes that have similar spectral characteristics, such as roof and road, water and marsh. The overall classification errors, especially the false positive errors, are reduced by up to 50%. Moreover, by using the lidar elevation data, the classification results show more realistic and homogeneous distribution of geographic features. This property will benefit the subsequent vectorization of the classification maps and the integration of the vector data into a geographical information system.

Keywords lidar, satellite image, classification, coastal mapping

Costal zone mapping (or in short, coastal mapping) has been a major application field for modern surveying and mapping technologies. As a rapid, efficient, and cost-effective representative of these technologies, multispectral (including hyperspectral) remote sensing imagery and laser altimetry (or bathymetry) are of the primary interest for both theoretical study and practical applications. The use of multispectral images for coastal mapping is, in general, based on image classification principles. Braud and Feng (1997) utilize the popular Landsat TM imagery for semiautomatic coastline reconstruction. Studies on the use of airborne hyperspectral images are presented by Nichols et al. (2000) using Airborne Terrestrial Applications Sensor (ATLS, 14 bands), by Siciliano et al. (2000) using HyMap sensor (126 bands), and by Lee et al. (2000) using Airborne Visible-Infrared Imaging Spectrometer (AVIRIS, 222 bands). These airborne images are at a higher spatial resolution of 1–3 meters and a higher spectral resolution with a minimum of 14 bands. They provide not only more accurate cartographic products but also detailed information

Received 28 January 2002; accepted 20 June 2002.
Address correspondence to Jie Shan, Department of Geomatics Engineering, School of Civil Engineering, Purdue University, West Lafayette, IN 47907-1284. E-mail: jshan@purdue.edu

about the human-nature interaction process and its effects. As another advanced technology, airborne laser altimeter along with the on-board GPS (Global Positioning System) and INS (Inertial Navigation System) can provide the three-dimensional (3-D) location of the laser beam footprint on the ground or water bottom. Equipment with multiple return capability is able to separate water surface from water bottom in such a way that laser bathymetry becomes possible. Irish and Lillycrop (1999) present the technical principles of the SHOALS (Scanning Hydrographic Operational Airborne Lidar Survey) system and the experience gained in coastal mapping over the past years. Successful applications of this system in U.S. coastal mapping can be found at http://shoals.sam.usace.army.mil/ (online).

However, no single type of data can provide reliable and automatic solutions to a complicated mapping task. Misclassification often exists among spectrally similar materials such as (building) roofs and roads, or water and marsh. Therefore, inclusion of additional independent information is needed, which leads to image fusion as described in Pohl and van Gendern (1998). Our study is focused on the combination of IKONOS images and lidar data. This is motivated by the following three reasons. First, current IKONOS-2 satellite imagery provides a high resolution of up to one meter which is compatible with airborne remote sensing data. Therefore, the combined use of those two data sources could potentially benefit each other. Recent study (Dial 2000) shows that IKONOS images can be used to produce large-scale topographic maps at the scale of 1:4,800. Li et al. (2000) report their study using simulated IKONOS panchromatic images for precision positioning with focus on coastline mapping application. Second, airborne lidar data has become one of the most effective data sources for topographic mapping. The National Ocean and Atmospheric Administration (NOAA) has been using lidar technology over the last few years to collect elevation data to document the topographic changes along the shorelines. Under this mission, lidar data has been collected for a large percentage of the east and west shorelines in the U.S. and made available to the public at http://www.csc.noaa.gov/crs/tcm/index.html (online). Third, the different nature of the lidar and image data will provide information complementary to each other. Lidar data in nature are geometric range measurements, while IKONOS imagery records the spectral reflectance of the ground. Therefore, the combination of these two will provide both geometric and spectral information about the ground which otherwise will not be available. A recent study from Smith et al. (2000) presents the concept and system composition for fusing their compact hyperspectral images and SHOALS bathymetry/altimetry data for coastal mapping applications. With this integrated system, it is expected that more complete hydrographic surveys can be achieved more efficiently than with traditional single sensor-based approaches (Smith et al. 2000). Similar research using airborne lidar data and airborne color images have been reported (Park et al. 2001), where lidar elevation and intensity data are used as additional bands to participate in the classification of color images. It is concluded that the best classification can be achieved by using the combination of red image, lidar elevation, and lidar intensity.

This article will study the combination of airborne lidar altimetry data with IKONOS multispectral images and its benefit in the classification for coastal mapping applications. The study area is located at Camp Lejeune, North Carolina and its surroundings. We will first show that the use of properly preprocessed lidar data will enhance image appearance and thus benefit the training site selection process, which is highly operator-dependent and perceptual in image classification. A class schema of six classes is then chosen for mapping purpose over this coastal area. Next, supervised image classifications are carried out with and without the use of lidar data, respectively. In order to evaluate and compare the classification results, we present detailed statistics represented by the confusion matrix and

overall accuracy indices. Comparative graphics are presented to illustrate the benefit gained in fusing lidar data with IKONOS images. It is concluded that the inclusion of the lidar data can significantly reduce the false alarm rate in image classification, greatly improve the separation of spectrally similar features, such as water and marsh, or roof and road, which would otherwise be misclassified. It is also found that by using the lidar elevation data the classification results present a more realistic and homogeneous distribution of geographic feature classes.

The remaining part of this article is organized as follows. The next section presents a brief introduction of the IKONOS images and lidar data used in this study. Class schema and supervised classification results along with graphic and tabular samples obtained with and without the use of lidar data are shown in the sections which follow the data section. This provides an intuitive and comprehensive evaluation on the classification results. There, a thorough analysis, based on the resultant statistics, is presented with quantitative comparisons and elaboration. The final section summarizes the article with concluding remarks and a prospect on future efforts.

Data for the Study Area

The study area is located along the coastal area south of Camp Lejeune, North Carolina, and multiple IKONOS panchromatic and multispectral images of the entire region are available. However, only a narrow strip of airborne lidar data along the Atlantic coast is available for this study. The common area (about 10.1×8.1 square km) covered by both IKONOS images and the lidar data was used for our study. Figure 1 displays the multispectral IKONOS images with IR (infrared) band for red channel, green band for green channel, and blue band for blue channel, whereas the lidar elevation data is displayed as a black and white image. The properties of IKONOS image and lidar data are listed below.

IKONOS multispectral images:

- Spectral resolution—4 bands (Near IR/R/G/B), 11 bits/pixel;
- Spatial resolution—4 meters $\times$ 4 meters/pixel (trimmed to 2521 $\times$ 2028 pixels);
- Preprocessing from Space Imaging, Inc.—Standard Geometrically Corrected, Mosaicked;
- Horizontal positional accuracy (root mean square error)—25 meters; and
- Map projection—UTM Zone 18, WGS-84.

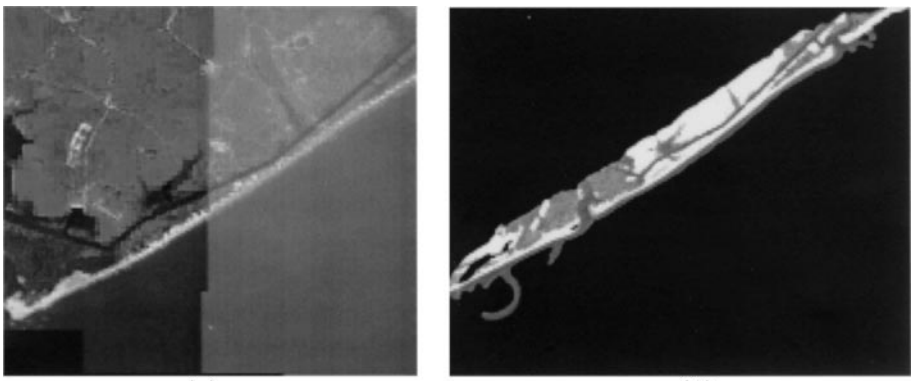

FIGURE 1 Data for the study area: (a) IKONOS, (b) lidar elevation.

Lidar elevation data:

- Spatial resolution (cell size)—3 m $\times$ 3 m;
- Horizontal positional accuracy—The ATM (Airborne Topographic Mapper) lidar elevation points are known to be horizontally accurate to $+/-$ 0.8 m at an aircraft altitude of 700 m;
- The ATM lidar elevation measurements have been found to be within $+/-$ 15 cm of each other in successive and overlapping passes of the same area;
- Map projection—UTM Zone 18, WGS-84; and
- Elevation reference—The vertical values in this data set have been converted to reference NGVD29, using the VERTCON software provided by the National Geodetic Survey.

Fusion and Classification

The supervised classification involves the design of class schema, selection of training sites, selection of checking (test) sites, and assessment of the classification results. This section will present the IKONOS image classification results and statistics for the with-lidar and without-lidar cases.

Fusion

The inclusion of lidar data into IKONOS imagery attempts to benefit the visual selection of training sites and to improve the quality of the classification. Unlike existing methods that include the digital elevation data in a postclassification process (Bolstad and Lillesand 1992; Harris and Ventura 1995), for which a series of rules have to be established and extra postprocessing steps are needed, we propose to use the lidar elevation within the classification process.

The lidar data must be preprocessed before it can be fused with IKONOS images. First, it is resampled to the same ground sample interval as the IKONOS images, namely resampled from 3 m to 4 m cell size. Second, the lidar data is linearly stretched to map its original elevation range (-1 to 38.4 m) to the 11-bit data range of the IKONOS images (0–2047). To display the lidar data along with the IKONOS images, we use IKONOS NIR band for red channel, green band for green channel, and processed lidar data for blue channel. The registration of lidar and IKONOS data needs to be evaluated before classification as any misregistration among the participant data may affect the classification quality. To do so, we measured six evenly distributed feature points on the lidar data and IKONOS image. These features include road intersection, house corner, bridge corner, and distinct point feature. The standard deviation of the positional differences for those six feature points is 0.61 pixel on the image (1 pixel $=$ 4 m). Therefore, it is concluded that the lidar data and IKONOS image are well coregistered and no further registration refinement is applied. A portion of the original IKONOS image and the fused result are shown in Figure 2. The four-band IKONOS image and the processed lidar data over the same area are then stored as a five-band multispectral image containing IKONOS NIR, red, green, blue band, and the lidar elevation data for the following classification operation.

Supervised Classifications

As shown in Figure 1, the test area contains a large percentage of water bodies as well as a variety of other geographic features in a coastal area. In order to design the class schema, namely, to determine what classes should be used for the study, an unsupervised

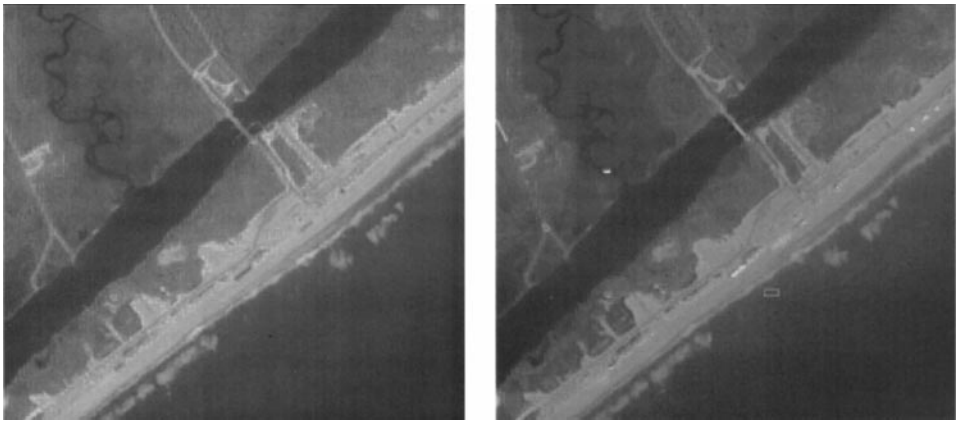

FIGURE 2 IKONOS image (left) and its fusion with lidar elevation (right).

classification (clustering) based on the ISODATA (Iterative Self-Organizing Data Analysis Techniques Algorithm) (Mather 1999) is carried out. A maximum of 12 clusters is specified for the clustering. A visual inspection of the clustering results leads to six primary classes: Road, Water, Marsh, Roof, Tree, and Sand. The class Road is used for roads comprised of grayish and white or bluish-white pixels. The class Roof is used for gray, white, and light blue rooftop pixels. The class Marsh is used for the reddish-brown areas adjacent to waterways.

The supervised classifications are then performed respectively for the original IKONOS four-band images and the five-band combined images using the maximum likelihood classifier (Landgrebe 2000; Mather 1999). To do so, evenly distributed pixel groups of above selected six classes need to be selected as training sites. These training sites are used by the classifier as a reference to calculate the class statistics that are then used to assign each pixel in the image to a corresponding class category (Biehl and Landgrebe 2002). In order to evaluate the classification results, a number of checking sites are also selected. The pixels in the checking sites do not contribute to the training and classification process. Instead, they are used as ground truth to check the classification results. In our study, the training sites and checking sites are selected visually in the fused data set. Some of the selected training sites are shown by the small white rectangles on the fused image in Figure 2. Classifications are carried out, respectively, without and with the lidar data. For comparison purposes, both classifications use the same training sites and checking sites. Table 1 lists the number of

TABLE 1 Number of Pixels for Training and Checking Sites

	Number of pixels	
Class name	Training sites	Checking sites
Road	120	164
Water	494	594
Marsh	142	156
Roof	53	42
Tree	210	208
Sand	102	182
Total	**1121**	**1346**

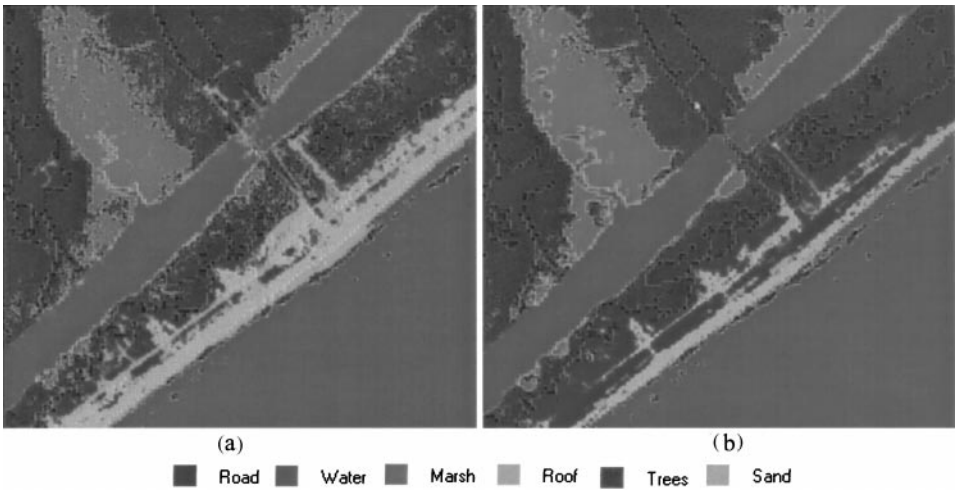

FIGURE 3 Comparison of classification results: (a) without lidar, (b) with lidar.

pixels selected for training sites and checking sites. Figure 3 presents a zoomed-in portion of the two classification results. The complete statistics for the classification results are tabulated in Tables 2 and 3.

Analysis and Evaluation

Table 2 contains all the primary statistics for the classification results presented in the form of the confusion matrix (Mather 1999; Smits et al. 1999). Its first column gives the class names of the ground truth, followed in the second column by the number of pixels selected either in the training sites (Table 2a) or checking sites (Table 2b) of a class. The third to eighth columns are the number of pixels identified by the classifier as the corresponding classes. The diagonal elements of the confusion matrix contain the number of pixels that are correctly labeled by the classifier, while the off-diagonal elements stand for the number of wrongly labeled pixels. Ideally, a perfect classification should yield a confusion matrix with all off-diagonal elements equal to zero and diagonal elements equal to the number of pixels of each ground truth class. The last column in the table, accuracy, is the percentage of the correctly labeled pixels in a ground truth class. It is essentially the ratio of a diagonal element over the number of pixels of the corresponding ground truth (the second column). The ninth row of the table, reliability, describes another quality index for the classification outcome. It is defined as the percentage of correct pixels in a labeled class. It is in fact the ratio between a diagonal element and the number of pixels in the corresponding identified class (the eighth row). These definitions are expressed in Equations (1) and (2). In order to present an overall quality index, the algebraic averages for accuracy and reliability for all six classes are listed in the last row of the table.

$$\text{Accuracy for class } i(\%) = \frac{\textit{number of correctly identified pixels in class } i}{\textit{total number of pixels in class } i}; \quad (1)$$

$$\text{Reliability for class } i(\%) = \frac{\textit{number of correctly identified pixels in class } i}{\textit{total number of pixels in the labeled class } i}. \quad (2)$$

To facilitate the analysis and visualize the classification quality, we further define two types of classification errors associated with accuracy and reliability. The first one is omission or

TABLE 2 Confusion Matrix of the Classification Results

Class name	Number pixels	Number of pixels in classification results (without/with lidar)						Accuracy (%)
		Road	Water	Marsh	Roof	Tree	Sand	
a. Training sites								
Road	120	117	0	0	1/0	0	2/3	97.5
Water	494	0	494	0	0	0	0	100.0
Marsh	142	0	0	141/142	0	1/0	0	99.3/100.0
Roof	53	3/0	0	0	49/53	0	1/0	92.5/100.0
Tree	210	0	0	0	0	210	0	100.0
Sand	102	1/0	0	0	1/0	0	100/102	98.0/100.0
Total	1121	121/117	494	141/142	51/53	211/210	103/105	
Reliability (%)		96.7/100.0	100.0	100.0	96.1/100.0	99.5/100.0	97.1	
Average accuracy (%): 97.9/99.6					Average reliability (%): 98.2/99.5			
b. Checking sites								
Road	164	137/146	0	0	11/0	0	16/18	83.5/89.0
Water	594	0	567/569	27/0	0	0/25	0	95.5/95.8
Marsh	156	0	0	113/124	0	43/32	0	72.4/79.5
Roof	42	0	0	0	39/42	0	3/0	92.9/100.0
Tree	208	3/0	0	0	0	205/208	0	98.6/100.0
Sand	182	2/7	0	0	0	0	180/175	98.9/96.2
Total	1346	142/153	567/569	140/124	50/42	248/265	199/193	
Reliability (%)		96.5/95.4	100.0/100.0	80.7/100.0	78.0/100.0	82.7/78.5	90.5/90.7	
Average accuracy (%): 90.3/93.4					Average reliability (%): 88.1/94.1			

Note: In the above tables, each cell lists two resultant values obtained from the classifications without and with lidar data. The format is *without lidar value/with lidar value*. If only one value exists, then it applies to both classification results. Detailed explanations can be found in the section of this article on analysis and evaluation.

TABLE 3 Error Matrix of the Classification Results

	Training sites		Checking sites	
Class	Omission (FN, %)	Commission (FP, %)	Omission (FN, %)	Commission (FP, %)
Road	2.5	3.3/0.0	16.5/11.0	3.5/4.6
Water	0.0	0.0	4.5/4.2	0.0
Marsh	0.7/0.0	0.0	27.6/20.5	19.3/0.0
Roof	7.5/0.0	3.9/0.0	7.1/0.0	22.0/0.0
Tree	0.0	0.5/0.0	1.4/0.0	17.3/21.5
Sand	2.0/0.0	2.9/2.9	1.1/3.8	9.5/9.3
Average	2.1/0.4	1.8/0.5	9.7/6.6	11.9/5.9

Note: In the above table, each cell lists two resultant values obtained from the classifications without and with lidar data. The format is *without lidar value/with lidar value*. If only one value exists, then it applies to both classifications. FN: False negative; FP: False positive or false alarm.

false negative (FN) error, which means the percentage of wrongly labeled pixels in a given ground truth class. The second one is commission or false positive (FP or false alarm) error, which stands for the percentage of wrongly labeled pixels in an identified class. They can be calculated with the following formulas:

$$\text{Omission (\%) or false negative for class } i = 100\% - \textit{accuracy for class } i; \quad (3)$$

$$\text{Commission (\%) or false positive for class } i = 100\% - \textit{reliability for class } i. \quad (4)$$

In a similar way, the average omission and average commission can be respectively defined as the average of omission (FN) and commission (FP) errors for all the classes. Using Equations (3) and (4) the two types of errors in the classifications for both without and with lidar data are calculated in Table 3, which is then charted as shown in Figure 4.

As shown in Table 3 and Figure 4, proper inclusion of the lidar data can reduce the omission (FN) and commission (FP) errors for almost all the classes and the overall error

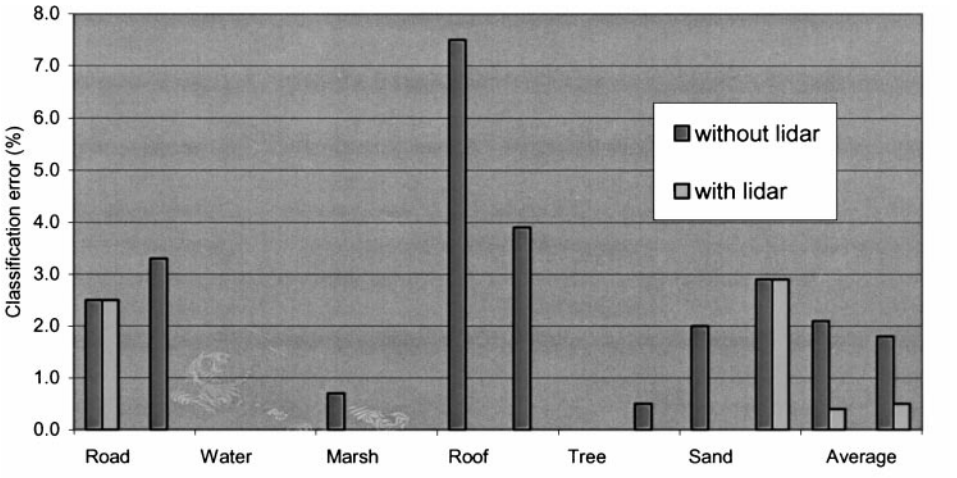

FIGURE 4a Classification errors of training sites for each class. The left two bars are omission error, the right ones are commission error.

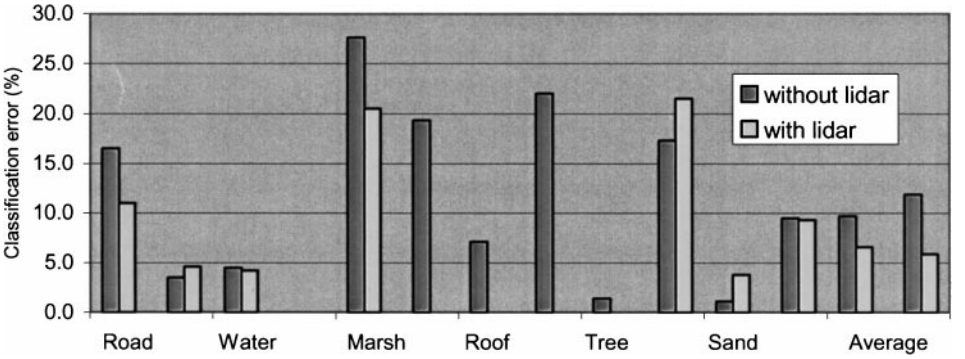

FIGURE 4b Classification errors of checking sites. For each class, the left two bars are omission error, the right two ones are commission error.

rates are remarkably reduced, which means both classification accuracy and reliability are improved. As shown in Figure 4a, the inclusion of lidar data greatly reduces classification errors of almost all training sites and no deterioration occurs. For some training sites, classification errors vanish (no vertical bars are shown in the chart). As for checking site errors, Figure 4b shows the classes that most benefited from the combination of lidar and IKONOS images are roof, marsh, and road. Roofs can be totally correctly (accuracy) classified and separated (reliability) from other classes. The omission and commission errors for roofs have vanished. As for the marsh class, omission error is reduced about 7% (from 27.6% to 20.5%) when lidar data is used; while commission error is eliminated (from 19.3% to 0), which means no nonmarsh pixels are wrongly labeled as marsh class. For the road class, Table 3 and Figure 4b show the use of lidar data causes about 5% more road pixels correctly labeled (error rate from 16.5% to 11.0%). As a result of using lidar data, the average false negative error is reduced from 9.7% to 6.6%, and 11.9% to 5.9% for the average false positive error, which means a significant 50% drop of the error rate.

Perhaps the most significant benefit of including lidar in the classification is the improved separability between roof and road classes. Since both roof and road are often composed of asphalt materials, they can have similar spectral characteristics that make discrimination more difficult if only IKONOS images are used. Misclassification between road and roof pixels is a common experience. The ability to separate two similar materials is also influenced by the number of spectral bands available. Having too few spectral bands means that the spectral space may have too few dimensions to separate similar materials. Thus in the case of IKONOS imagery, the misclassification problem is intensified due to the difficulty in separating similar materials using only four spectral bands. Adding lidar data as an independent and heterogeneous data source improves the discrimination between roof and road significantly. As shown in Table 2b for the multispectral-only classification of checking sites, the reliability accuracy for the roof class is 78%. Of the roof pixels that are misclassified, all are incorrectly assigned to the road class. With the addition of lidar data as the fifth band, reliability accuracy improves from 78% to 100% for the roof class. The accuracy improvement in roof classification has important ramifications for feature extraction algorithms guided by thematic classes. By eliminating misclassification between road and roof, a better initial approximation to building delineations is achieved and false positives are drastically reduced (Lee et al. 2002).

Although a downside of combining lidar data with IKONOS images is found in this study, it is marginal. The use of lidar data causes more (from 17.3% to 21.5%) nontree pixels wrongly classified as the tree class. Table 2b reveals that these nontree pixels are actually

water and marsh pixels, which suggests a certain separability problem among these three classes. A similar effect is also observed in road and sand classes. This is likely caused by the insufficient horizontal and vertical resolution of the lidar data such that it cannot contribute to the separation of the classes that may not be distinct in elevation. Accordingly, the simple inclusion of the lidar data in the classification without properly considering its accuracy and its topographic properties, such as average elevation, slope, and aspect, may degrade the results for these classes. It should be noted that this minor degradation is consistent with earlier findings in image classification studies. It has long been known that that the classification quality may decrease if more bands are included in the conventional classification process (Hughes 1968; Shahshahani and Landgrebe 1994). To overcome this so-called Hughes effect or phenomenon, certain preprocessing needs to be performed to select features or subspace in the original data before classification. However, this topic is not within the scope of our current study and will be addressed elsewhere in the future.

Since the above quantitative analysis cannot show the pattern and distribution of errors of the geographic features in the classification results, an evaluation based on the classified thematic maps is necessary. Compared to Figure 2, the roof class (in yellow) in Figure 3b is located at the actual building rooftops, while in the IKONOS-only map areas of the beach, the road and bridge crossing the intercoastal waterway and several other areas that are not rooftop are misclassified as roof. The effect is that the yellow pixels in Figure 3a present an unrealistic pattern and distribution of roofs. A similar observation can also be made about the water, marsh, and tree classes. Furthermore, a comparison of the two maps in Figure 3 indicates that the water, marsh, tree, and sand classes in Figure 3b show a more realistic and homogeneous distribution than in Figure 3a. The “salt and pepper” scattering effect of isolated pixels in Figure 3a is significantly removed in Figure 3b when lidar data is used. Semantic conflicts, such as a small number of roof pixels surrounded by roads, marsh by water and trees, and roofs by sand, are limited. This more realistic distribution will certainly benefit the subsequent vectorization process in costal mapping and vector database integration.

Conclusions

The complexity of coastal mapping tasks requires the combination of multiple, independently collected, and preferably heterogeneous remote sensing data. Recently available high-resolution satellite imagery makes it possible and beneficial to merge the imagery with lidar elevation data for coastal classification mapping. It is shown that, via simple preprocessing, the lidar elevation data can be treated as an extra band to be combined with multispectral IKONOS images. The integration significantly improves the classification accuracy and reliability of geographic feature classes with similar spectral characteristics, such as roof and road, water and marsh. By including lidar data, the average classification errors, especially the false positive (commission) errors, are reduced by as much as 50% (from 11.9% to 5.9%). Moreover, the classification results of the lidar-enhanced data show much more realistic and homogeneous distribution of geographic features than the without-lidar results. This property will benefit the subsequent vectorization of the classification maps and the integration of the vector data into a geographical information system. A Hughes effect is observed in this study in that the classification error (from 17.3% to 21.5%) for the tree class is slightly increased due to its mixture with marsh and water. Future studies will be focused on a modified use of lidar data to take into consideration the local terrain properties, such as average elevation, slope and aspect, and thus benefit the separation of geographic feature classes at both similar and different elevations.

References

Biehl, L., and D. Landgrebe. 2002. MultiSpec: A tool for multispectral-hyperspectral image data analysis. *Computers & Geosciences* 28(10):1153–1159.

Braud, D. H., Jr., and W. Feng. 1997. Semi-automated construction of the Louisiana coastline digital land/water boundary using Landsat thematic mapper satellite imagery. Department of Geography & Anthropology, Louisiana State University, Technical Report Series, 97-002. Available at http://www.osradp.lsu.edu/1997_Deliverables/Braud97/Braud97.htm

Bolstad, P., and T. Lillesand. 1992. Rule-based classification models: Flexible integration of satellite imagery and thematic spatial data. *Photogrammetric Engineering and Remote Sensing* 58(7):965–971.

Dial, G. 2000. IKONOS Satellite Mapping Accuracy. CD-ROM. Proceedings of the ASPRS Annual Conference, Washington, D.C., May 22–26.

Harris, P., and S. Ventura. 1995. The integration of geographic data with remotely sensed imagery to improve classification in an urban area. *Photogrammetric Engineering and Remote Sensing* 61(8):993–998.

Hughes, G. 1968. On the mean accuracy of statistical pattern recognizers. *IEEE Transaction on Information Theory* IT-14(1):55–63.

Irish, J. L., and W. J. Lillycrop. 1999. Scanning laser mapping of the coastal zone: The SHOALS system. *ISPRS J. of Photogrammetry & Remote Sensing* 54(2–3):123–129.

Landgrebe, D. 2000. Information extraction principles and methods for multispectral and hyperspectral image data. In *Information Processing for Remote Sensing*, edited by C. H. Chen. River Edge, NJ: World Scientific Publishing.

Lee, D. S., J. Shan, and J. S. Bethel. 2002. Classification-guided building extraction from IKONOS imagery. CD-ROM. Proceedings of the ASPRS Conference, Washington, D.C., April 22–26.

Lee, Z. P., K. L. Carder, and F. R. Chen. 2000. Bathymetry and environmental properties observed from AVIRIS data. *Proceedings of the Sixth International Conference on Remote Sensing for Marine and Coastal Environments*. Charleston, SC, May 1–3.

Li, R., G. Zhou, S. Yang, G. Tuell, N. Schmidt, and C. Fowler. 2000. A study of the potential attainable geometric accuracy of IKONOS satellite imagery. 2000, CD-ROM. Proceedings of ASPRS Annual Conference, Washington, D.C., May 22–26.

Mather, P. M. 1999. *Computer processing of remotely-sensed images: An introduction*, 2nd Edition. United Kingdom: John Wiley & Sons.

Nichols, C., T. Siewicki, J. Daugomah, D. Porter, and B. Jones. 2000. Coastal landcover classification using NASA's Airborne Terrestrial Applications Sensor (ATLAS) data. *Proceedings of the Sixth International Conference on Remote Sensing for Marine and Coastal Environments*. Charleston, SC, May 1–3.

Park, Joong-Yong, R. L. Shrestha, W. E. Carter, and G. H. Tuell. 2001. Land cover classification using combined ALSM (LIDAR) and color digital photography. Paper presented at the ASPRS Annual Conference, St. Louis, April 23–27.

Pohl, C., and J. van Gendern. 1998. Multisensor image fusion in remote sensing: Concepts, methods and application. *International J. of Remote Sensing* 19(5):823–854.

Shahshahani, B., and D. Landgrebe. 1994. The effect of unlabeled samples in reducing the small sample size problem and mitigating the Hughes Phenomenon. *IEEE Transactions on Geoscience and Remote Sensing* 32(5):1087–1095.

Siciliano, D., D. Potts, B. Martini, E. Silver, and W. Pickles. 2000. High resolution hyperspectral remote sensing as an environmental monitoring tool for coastal margins. Sixth International Conference on Remote Sensing for Marine and Coastal Environments. Charleston, SC, May 1–3.

Smith, R. A., J. L. Irish, and M. Q. Smith. 2000. Airborne lidar and airborne hyperspectral imagery: A fusion of two proven sensors for improved hydrographic surveying, *Proceedings of Canadian Hydrographic Conference*, Montreal, Canada, May 15–19.

Smits, P., Dellepiane, and R. Schowengerdt. 1999. Quality assessment of image classification algorithms for land-cover mapping: A review and a proposal for a cost-based approach. *International J. of Remote Sensing* 20(8):1461–1486.